J Electr Eng Technol Vol. 9, No. 5: 1643-1653, 2014
http://dx.doi.org/10.5370/JEET.2014.9.5.1643

ISSN(Print) 1975-0102
ISSN(Online) 2093-7423

# Development of LED Street Lighting Controller for Wind-Solar Hybrid Power System

**Yong-Sik Lee* and Jae-Hyeon Gim†**

**Abstract** – This paper presents the design and implementation of a wind-solar hybrid power system for LED street lighting and an isolated power system. The proposed system consists of photovoltaic modules, a wind generator, a storage system (battery), LED lighting, and the controller, which can manage the power and system operation. This controller has the functions of maximum power point tracking (MPPT) for the wind and solar power, effective charging/discharging for the storage system, LED dimming control for saving energy, and remote data logging for monitoring the performance and maintenance. The proposed system was analyzed in regard to the operation status of the hybrid input power and the battery voltage using a PSIM simulation. In addition, the characteristics of the proposed system's output were analyzed through experimental verification. A prototype was also developed which uses 300[W] of wind power, 200[W] of solar power, 60[W] LED lighting, and a 24[V]/80[Ah] battery. The control system principles and design scheme of the hardware and software are presented.

**Keywords**: Wind-Solar hybrid power system (WS-HPS), LED street lighting, Battery charge-discharge, Dimming control

## 1. Introduction

In the last few years, renewable energy has experienced some of the largest growth of over 30% per year compared with the growth of coal and lignite energy [1]. In particular, wind power and solar power technologies have grown substantially among renewable energy technologies. Wind energy and solar energy are sustainable clean energy sources that can be used to address problems with increasing energy demands and environmental pollution worldwide. However, renewable energy is limited by environmental factors [2].

WS-HPS is currently used as a standalone system in remote mountainous regions and islands as well as in various applications such as traffic lights, streetlights, and wireless broadcasting [3]. The efficiency of WS-HPS is largely determined by the lifetime and storage capacity of the battery in the system. The battery lifetime and storage capacity are affected by inconsistent charging and discharging of the battery. In addition, low power consumption has become an important demand for WS-HPS. LED dimming control to reduce power consumption has become essential.

Maintenance is also important. Street lighting control system operators wish to reduce maintenance and repair costs. To facilitate this, streetlight control systems should have the ability to give information about operation and maintenance to the operators [4]. Efficient and reliable operation of WS-HPS largely depends on the control strategies of the controller, and remote monitoring.

This paper describes the design of the WS-HPS in four main aspects: a hybrid control strategy for the wind solar system with maximum power point trace, charging and discharging of the battery for increasing lifetime, LED dimming control for energy saving, and real-time monitoring to monitor the performance and for maintenance.

The proposed system has been designed to enable maximum power point tracking (MPPT) of the WP-HPS and efficient charge-discharge control of the battery. In addition, based on the input of an infrared (IR) sensor, LED street lighting dimming is controlled. This enhances the energy efficiency of the WP-HPS.

The remote monitoring of the WP-HPS has been developed using Zigbee modules. The development system has been analyzed in regard to the operation characteristics through PSIM simulation. A field experiment was also conducted for the control status of the system, as well as power management for the battery status and the characteristics of WP-HPS output based on insolation and wind speed.

## 2. System Configuration

A configuration diagram of the LED street lighting controller using the WS-HPS is shown in Fig. 1. This system uses a 300[$W$] wind generator, 200[$W$] photovoltaic modules, 24[$V_{dc}$]/60[$W$] LED street lighting, and a 24[$V_{dc}$]/100[$Ah$] battery. A DC-DC stage is also used to buck the higher voltage of the wind and solar to the lower DC

† Corresponding Author: Dept. of Electrical Control Engineering, Sunchon National University, Korea. (jhg@sunchon.ac.kr)
* Dept. of Electrical Engineering, Sunchon National University, Korea. (ys5675@sunchon.ac.kr)
Received: January 9, 2013; Accepted: May 31, 2014

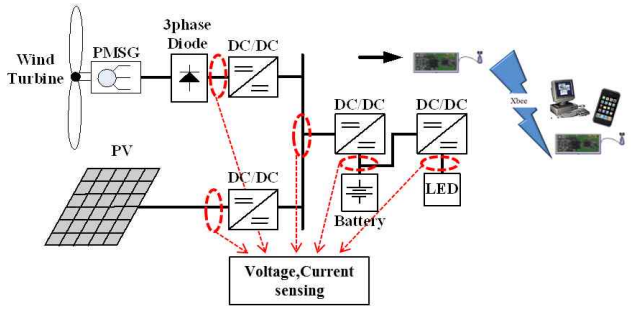


**Fig. 1.** Structure of the standalone WS-HPS

voltage of the battery and LED street lighting.

## 2.1 Design of WS-HPS

The system is a small and independent power system that is mainly composed of six major parts: the wind power system, solar power system, hybrid control system, battery charging system, LED lighting system, and main control system with communication.

### *2.1.1 Wind power system*

The wind power system consists of a wind turbine coupled with a permanent magnet synchronous generator (PMSG), generator breaking, a rectifier, and a buck converter. The specifications of the wind generator are shown in Table 1. The generator braking involves locking the rotor of the generator using a shunt resistor when the speed of the rotor is too high. The rectifier is a three-phase diode rectifier that is used to convert three-phase AC voltage to DC voltage. The buck converter is a DC-DC converter that the voltage input-output ratio is controlled by the duty ratio of the pulse width modulation (PWM) signal from the MPPT controller.

The reference voltage level of the wind power system MPPT is based on the battery voltage level. However, the wind power system and solar power system generate power at the same time, and the reference voltage level of the wind power system MPPT tracks the output voltage level of the solar power system. This is more effectively described in detail in section 2.2.2.

### *2.1.2 Solar power system*

The solar power system consists of a photovoltaic module and a buck converter. The photovoltaic module has an optimal operating voltage at which the photovoltaic module can produce maximum power. The specifications of the photovoltaic module are shown in Table 2.

**Table 1.** Specifications of wind generator

| Model | ED-300[W]/AC24[V] |
|---|---|
| Rating Voltage | DC 24[V] |
| Rating Current | 12.5[A] |
| Rating Speed | 1850[r/m] |
| Maximum Power | 380[W] |
| Starting Wind speed | 3.5[m/s] |
| Rating Wind Speed | 12.5[m/s] |
| Generator/Blade | PMSM/3ea |

**Table 2.** Specifications of photovoltaic module

| Model | SCM-100[W] |
|---|---|
| Maximum Power Voltage | 19.5[V] |
| Maximum Power Current | 5.4[A] |
| Open Circuit Voltage | 23.8[V] |
| Short Circuit Current | 5.8[A] |
| Insolation | 1000[W/m$^2$] |
| Air mass | 1.5 |
| Temperature | 25[°C] |

### *2.1.3 Hybrid control system*

This control system can be controlled to connect each voltage level of the wind-solar power system. The control circuit of the hybrid power system is shown in Fig. 2. The proposed controller structure is composed of step down (buck) converters with main switching devices, choke coil L, output smoothing capacitor C, gate driver, parasitic elements, and voltage-current sensors.

The half-bridge buck converters were designed with IRFB23N15DPBF MOSFETs ($V_d$= 150[$V$], $I_d$= 23[$A$], $R_{ds}$ =0.090[ Ω ], N-channel) after considering the input voltage, current, and internal resistance of the system. The converters also use FAN7382 gate drivers.

If the inductance of the converter increases in the circuit design, the ripple current flowing in the choke coil becomes smaller. The output ripple voltage requirements can be satisfied even if the capacity of the smoothing condenser is small. In addition, by considering that the smoothing condenser has the maximum allowable ripple current regulation, if possible, the ripple current of the choke coil should be small. If the inductance increases, the choke coil must be bigger, which will increase the price of the system.

The capacity calculation of the inductor can be represented by:

$$L = \frac{t_{on}}{\Delta I_{L(on)}}\left(V_{in} - V_{out}\right) \tag{1}$$

where $t_{on}$ and $\Delta I_{L(on)}$ are the on time of the duty ratio and inductor current variation magnitude, and $V_{in}$ and $V_{out}$ are the input and output voltage of system, respectively. Based on Eq. (1), the proposed system uses an inductor with a capacity of approximately 220[$uH$]/15[$A$].

The ripple current flowing in the choke coil mostly flows into the output smoothing capacitor. The specifications of the electrolytic condenser used as a smoothing condenser are considered by the calculation of the equivalent series resistance (ESR). The ESR calculation and condenser can be represented by [5]:

$$ESR[\Omega] \le \frac{V_R}{\Delta I_L} \quad (2)$$

$$C_L[F] \le \frac{\Delta I_{out} t_L}{\Delta V_{out}} \quad (3)$$

where $t_L$ and $\Delta V_{out}$ are the shift times and output voltage, and $\Delta I_{out}$ is the amount of variation of the load current. There is a need to increase the capacity of the output smoothing capacitor to suppress the fluctuations of the output voltage. Based on Eqs. (2-3), the system uses low-impedance capacitors with capacities of 470[$uF$] /100[$V$].

### *2.1.4 Battery charging system*

The battery charging system consists of a 24[$V$]/100[$Ah$] battery and a buck converter. The battery is the most common method of energy storage in standalone systems. The battery should operate with an optimized energy management strategy. A lead acid battery was used due to its low cost and availability. The buck converter is a DC-DC converter that is used to protect the battery. Three steps are performed to charge the battery more effectively, which are described in detail in section 2.2.3.

### *2.1.5 LED light system*

The LED lighting load of the system has 24[$V$]/60[$W$] LED lighting and a buck converter. The relationship between the current and voltage of the LED lighting is nearly exponential. The system is operated in day or night modes by solar voltage. In night mode, the operation of the LED lighting is controlled by an IR sensor. The control circuit of the LED lighting system is the same as that shown in Fig. 2, except for the inverse voltage limit diode.

Near the rated point, a small change in voltage would cause a much bigger change in current, and the margins of safety could even be exceeded. So, the accurate and constant current control is very important in driving LED lighting. The buck converter is a DC-DC converter. For LED lighting, the converter requires features such as high efficiency, low energy consumption, and long life. To save energy, dimming operation is applied in the LED lighting system. The minimum operating voltage of the LED street lighting is 17.0[$V$], and the controller controls the dimming with voltages in the range of 17.0-24.0[$V$] (0.4-2.5[$A$]).

### *2.1.6 Main control with communication system*

The main control system includes a display unit, a remote communication unit, and microprocessor, as shown in Fig. 3.

The display unit uses a text LCD that shows the status of the WS-HPS which display the voltage and the current of the systems. The remote communication unit using a Zigbee module that sends the data collected to a master processor. The Zigbee module is a Zigbee Pro series wireless network module from Digi-Maxstream, and is used for remote diagnosis of the power system. This module is communicates with the microprocessor using UART communication. The ATmega128 single-chip micro-processor is used as the main control chip. All algorithms

**Fig. 3.** Main controller for WS-HPS

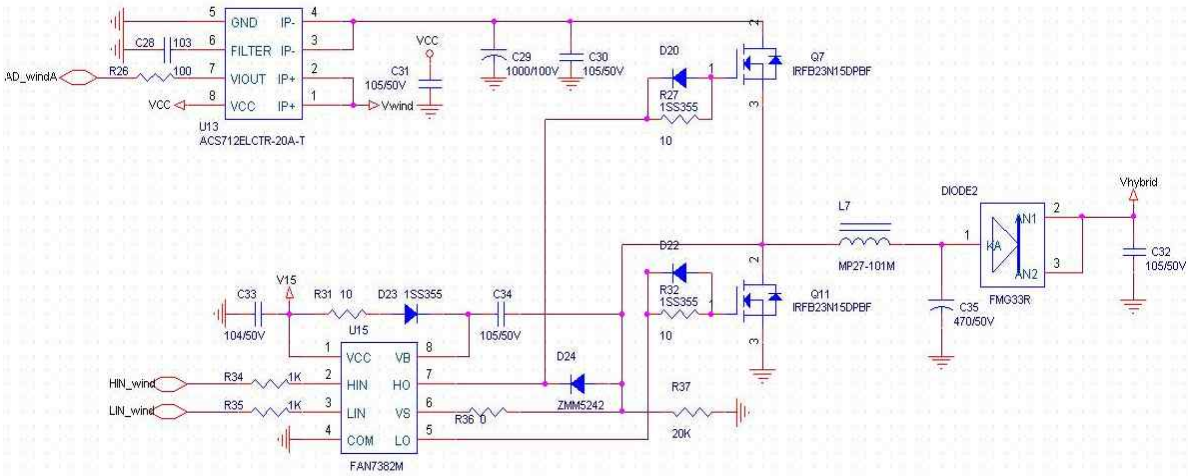


**Fig. 2.** Circuit of buck converter

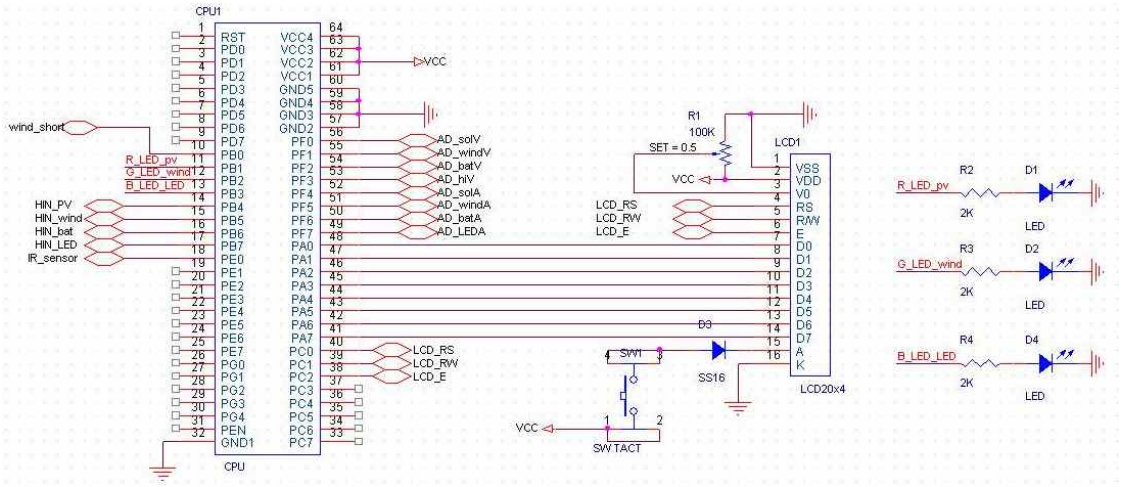


**Fig. 4.** Circuit of processor

to control the WS-HPS are implemented in this micro-processor. Sensors acquire current and voltage signals from the main circuit and are input into the control chip. The output signals of the control chip generate the gate signals of the MOSFET in the drive circuit.

Fig. 4 shows the input/output circuit of the ATmega128 processor used in this paper. The 8 A/D converter channels were used for sensing the voltages and currents of the wind-solar power system, battery system, and LED street lighting system. The controller uses 4 PC-PWM channels with 30-KHz frequency for PWM control of the buck converters. 1 switch port is used for brake switching operation of the wind generator, and a UART port is used for wireless network communication.

The remote processor includes a master Zigbee module, as shown in Fig. 5. The master module sends the data to collect information from the main control system of WS-HPS. The remote computer connects to the master processor system by a USB cable. The master processor system searches all main control systems every 200[msec] to check for faults and collect real-time data to send to the remote computer.

The specifications of the LED street lighting controller of the WP-HPS are shown in Table 3.

**Fig. 5.** The master module

**Table 3.** Feature of controller

| | Detail specification |
|---|---|
| Input Power | 24[V]/500[W]/2 port |
| Main Voltage | 24[V] Base configuration/ select 12[V] |
| MPPT | ~95[%] |
| Wind generator protection | Electronic brake function |
| Temperature compensation | 24[mV/°C]-(Heatsink specification) |
| Precision | 24[V] ≤0.1[%]± 30[mV] |
| Max. output current | 24[V]/ 15[A] |
| Output voltage(load) | 24[V]/ Dimming control(60~99[%])/ 1 port |
| Self current consumption | Self current consumption = 30[mA]<br>Include(IR sensor and LCD) = 100[mA] |
| Remote communications | XBee Pro (~4[km])<br>Remote fault diagnosis and control |

## 2.2 Software algorithm

The software of the control system is divided into two parts; the control algorithm and monitoring.

### *2.2.1 Main control algorithm*

The control algorithm is divided into four parts: day/ night setting, dimming control of the LED lighting, MPPT of the wind-solar power system, and battery charging-discharging. Fig. 6 shows a flowchart of the control algorithm, which is implemented through a microcontroller. In the proposed algorithm, the wind generator voltage $V_{wind}$, photovoltaic module voltage $V_{pv}$, battery voltage $V_{batt}$ are detected as feedback signals.

The wind generator is protected by calculating the wind speed. The day and night modes of the system are determined by whether $V_{pv}$ is greater or less than 5.5[$V$]. In night mode (when $V_{pv}$ is under 5.5[$V$]), the MPU checks for low battery voltage in order to protect the battery and to use the LED lighting. The LED lighting has a dimming function that is controlled by an IR sensor. If the battery voltage level is low, the LED lighting turned off, and the battery is charged.

The MPPT of the wind-solar power system is controlled

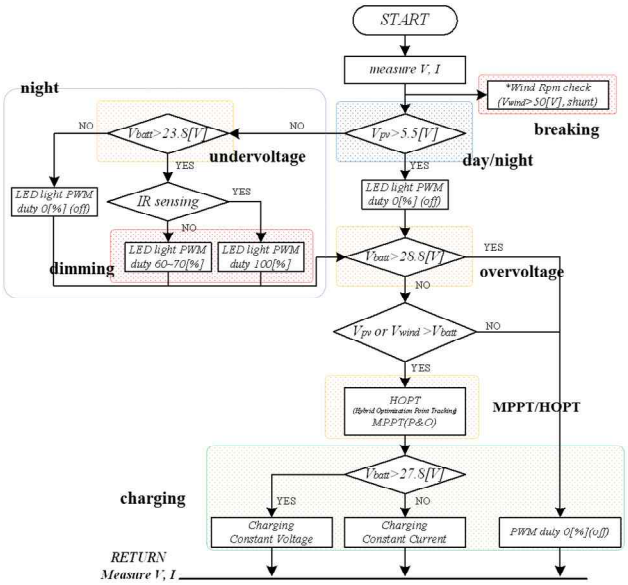


**Fig. 6.** Flowchart of control algorithm

by the HOPT (Hybrid Optimization Point Tracking) algorithm. Also, according to the different voltage levels of WS-HPS and the battery status, the charging and discharging range is monitored, and a flag bit is set.

### *2.2.2 HOPT(Hybrid Optimization Point Tracking)*

The HOPT control is used for extracting the optimization voltage and maximum power from the WS-HPS. The HOPT algorithm is described in the flowchart shown in Fig. 7.

This algorithm is divided into cases of dual input and single input. With single input, the power of input is controlled by only MPPT. In the case of dual input, the lower power in the dual input power is controlled by MPPT, and the other input power is tracks the voltage of the lower power.

The MPPT controller uses the Perturb and Observe (P&O) technique. This method is the most common algorithm in use because of its simplicity and low-cost implementation [6]. It only measures the voltage and current of the photovoltaic modules. P&O captures the maximum power point by perturbing the operating voltage, and calculates the output power at that point, which is compared with the previous value. After that, it increases ($V_{ref}$ + *step*) or decreases ($V_{ref}$ - *step*) the voltage until it reaches the maximum output power, where $dP/dV$=0 [7]. In this paper, a step value from 0.0005 to 0.001 is applied.

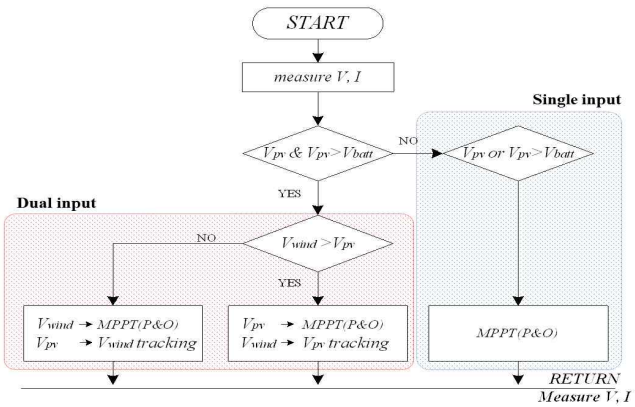


**Fig. 7.** HOPT Algorithm

The P&O algorithm operates by varying the duty cycle of the buck converter, thus varying the output voltage of the wind generator or photovoltaic modules. The resulting power is observed to increase or decrease the duty cycle in the next iteration. Fig. 8 shows how the P&O method works.

The specific control diagram of the WS-HPS is shown as Fig. 9. The voltage command ($V_{pv}^*$, $V_{wind}^*$) is determined by the HOPT algorithm, and an amplitude signal of voltage error ($V_{pverr}$, $V_{winderr}$) is obtained from the real voltage error signal between the voltage command ($V_{pv}^*$, $V_{wind}^*$) and voltage measurement ($V_{pv}$, $V_{wind}$) of the WS-HPS system. The system uses digital control, in order to enhance the control of dynamic and steady-state performance, uses proportional-integral(PI) controller to achieve the stable control loop, and got the PWM duty cycle (*PV_PWM*, *Wind_PWM*) through PI control.

### *2.2.3 Battery charging*

For battery charging, this controller uses the three-step charging algorithm shown in Fig. 10 [8, 9].

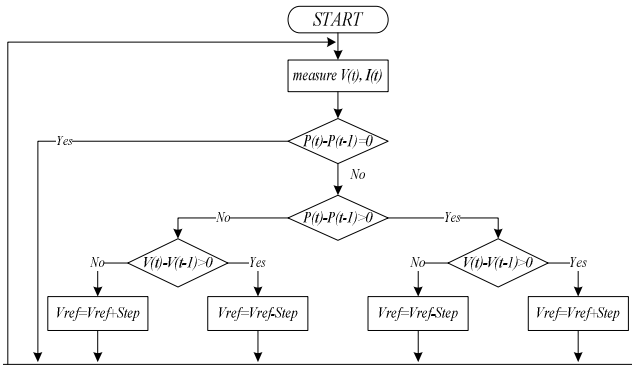


**Fig. 8.** P&O MPPT algorithm

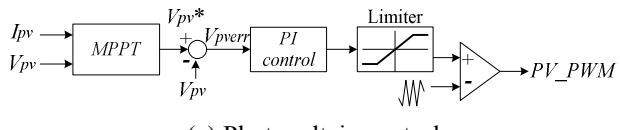


(a) Photovoltaic control

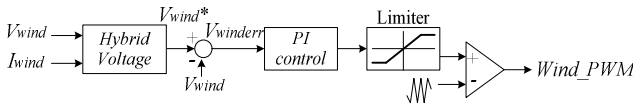


(b) Wind power generation control

**Fig. 9.** WS-HPS PWM control

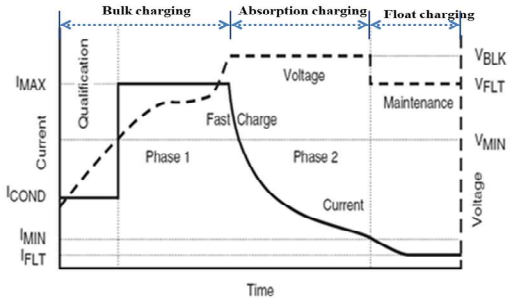


**Fig. 10.** Three step charging algorithm

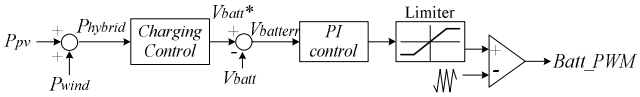


**Fig. 11.** Battery charging PWM control

The first step is bulk charging (constant current charging). The battery is charged at maximum current ($I_{MAX}$) using maximum power point tracking until the battery reaches its final charging voltage, which is known as the absorption voltage. This step replaces 70-80[%] of the battery's capacity at the fastest possible rate. The battery is kept in this mode until the charge voltage reaches the upper voltage threshold ($V_{BLK}$), typically 27.8[$V$].

The second step is absorption charging (constant voltage charging). While the battery voltage is maintained at the absorption voltage, the charging current is steadily decreased until its minimum current ($I_{MIN}$). This step replenishes the remaining 20-30[%] of the capacity.

The final stage is float charging. A small current is supplied to the battery to maintain the battery voltage ($V_{FLT}$). The overcharging current induces water loss at the negative electrode of the battery and grid corrosion at the positive electrode, which have a detrimental effect on the service life of the battery.

The control diagram for the precise control of battery charging and protection is shown Fig. 11. The controller for battery charging is operated by the combination of solar power ($P_{pv}$) and wind power ($P_{wind}$), and the voltage command ($V_{batt}^{*}$) is obtained by the three-step charging algorithm. The voltage error ($V_{batterr}$) that is obtained by comparing with battery voltage ($V_{batt}$) and voltage command ($V_{batt}^{*}$) can be obtained duty cycle such as Batt_PWM using PI controller.

### *2.2.4 LED lighting algorithm*

For saving energy, the LED lighting works with half luminance or less when there are no passers-by. Dimming of the LED lighting is essential for these purposes [10]. In the LED lighting system, the infrared sensor (IR sensor) detects the movement of people.

Fig. 12 shows the LED dimming controller. When the IR sensor is not activated, the LED lighting is dimmed by changing the current of the LED through modulating the

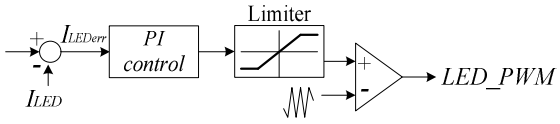


**Fig. 12.** Control of LED dimming

duty cycle of PWM signal. Taking the LED current as feedback, PI controller is applied to output constant current to the LED. When the infrared sensor senses a person, the maximum operating current of the LED lighting $I_{ref}$ is 5.0[$A$]. Otherwise, $I_{ref}$ is approximately 1.2[$A$]. If the IR sensor does not detect anything for 20 minutes, $I_{ref}$ is set to 0.5[$A$], which is the lowest operating current of the LED lighting.

### *2.2.5 Remote monitoring*

The remote computer application software employs multithreading technology written in Visual Studio C++, which provides the measurement and control system. The computer application software includes two threads. One thread provides functions for the data collection on the background.

The display on the screen shown in Fig. 13(a) has several functions that select the WS-HPS using Port set, monitor the current, voltage, and power of every system and log the data collected. The data logger interfaces with a

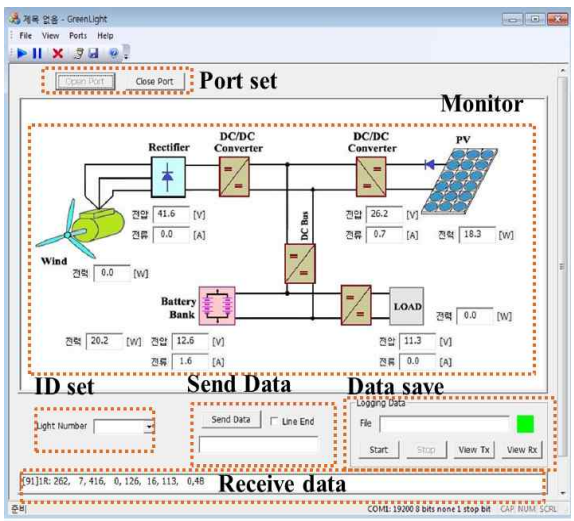


(a) Display on the screen

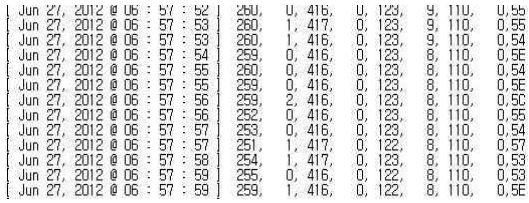

| | | | | | |
|---|---|---|---|---|---|
| Jun 27, 2012 @ 06 : 57 : 52 | 260, | 0, 416, | 0, 123, | 9, 110, | 0,55 |
| Jun 27, 2012 @ 06 : 57 : 53 | 260, | 1, 417, | 0, 123, | 9, 110, | 0,55 |
| Jun 27, 2012 @ 06 : 57 : 53 | 260, | 1, 416, | 0, 123, | 9, 110, | 0,54 |
| Jun 27, 2012 @ 06 : 57 : 54 | 259, | 0, 416, | 0, 123, | 8, 110, | 0,5E |
| Jun 27, 2012 @ 06 : 57 : 55 | 260, | 0, 416, | 0, 123, | 8, 110, | 0,54 |
| Jun 27, 2012 @ 06 : 57 : 55 | 259, | 0, 416, | 0, 123, | 8, 110, | 0,5E |
| Jun 27, 2012 @ 06 : 57 : 56 | 259, | 2, 416, | 0, 123, | 8, 110, | 0,5C |
| Jun 27, 2012 @ 06 : 57 : 56 | 252, | 0, 416, | 0, 123, | 8, 110, | 0,55 |
| Jun 27, 2012 @ 06 : 57 : 57 | 253, | 0, 416, | 0, 123, | 8, 110, | 0,54 |
| Jun 27, 2012 @ 06 : 57 : 57 | 251, | 1, 417, | 0, 122, | 8, 110, | 0,57 |
| Jun 27, 2012 @ 06 : 57 : 58 | 254, | 1, 417, | 0, 123, | 8, 110, | 0,53 |
| Jun 27, 2012 @ 06 : 57 : 59 | 255, | 0, 416, | 0, 122, | 8, 110, | 0,53 |
| Jun 27, 2012 @ 06 : 57 : 59 | 259, | 1, 416, | 0, 122, | 8, 110, | 0,5E |

(b) The data logger files

**Fig. 13.** GUI form and data logged for remote diagnosis

personal computer via USB. The software activates the data logger view and analyzes the collected data for verification of the performance of the WS-HPS based LED street lighting system

## 3. Simulation and Experiment

### 3.1 Simulation and results

The hybrid input / output analysis of the proposed system was simulated by PSIM, and the battery charger characteristics were analyzed. The simulation has four C blocks, and includes the wind power, solar power, and battery, as in Fig. 14. Wind speed and insolation have a close relationship with the power production of WS-HPS. Therefore, the characteristics of the proposed system were analyzed by changing these elements. The basic conditions of wind power and solar power are shown in Table 4.

The insolation and wind speed have been varied to analyze the photovoltaic and wind power output characteristics and MPPT control. In addition, the changes in the battery voltage for battery charging, constant voltage, and constant current characteristics were analyzed. Fig. 15 represents the system output characteristics. In Fig. 15(a) the wind speed was changed to 10[m/s] from 12[*m/s*], and in Fig. 15(b) the insolation was changed to 800[$W/m^2$] from 1000[*m/s*] under a battery voltage of 24[*V*].

At point (a) of Fig. 15(a), the wind speed changes. At this point, the output power and current of the wind generator were lowered to 110[*W*] from 300[*W*] and to 4.23[*A*] from 12.5[*A*], respectively. At point (b) of Fig. 15(b), the insolation changes. At this point, the output power and current of a photovoltaic modules were lowered to 60[*W*] from 100[*W*] and to 4.23[*A*] from 12.5 [*A*], respectively.

Fig. 15(c) illustrates the system output characteristics when changing the battery voltage to 28.0[*V*] from 23.8[*V*].

At point (c) of Fig. 15(c), the battery voltage is 26.9[*V*]. The battery is charged with constant voltage control at this point. 27.8[*V*] is the voltage at which the battery is completely charged. When the battery is fully charged, the input power switch of WP-HPS is turned off for battery overcharge protection.

**Table 4.** Feature of Photovoltaic / Wind generator

| Photovoltaic module | | Wind generator | |
|---|---|---|---|
| Model | ESN-50[W] | Model | ED-300[W] |
| Open Circuit Voltage | 21.0[V] | Rating Voltage/ Current | 24[V]/12.5[A] |
| Short Circuit Current | 3.60[A] | Maximum Power | 380[W] |
| Maximum Power Voltage | 17.5[A] | Starting Wind Speed | 3.5[m/s] |
| Maximum Power Current | 2.85[A] | Rating Wind Speed | 12.5[m/s] |
| 1000W/m$^2$, Air mass = 1.5, Temp. = 25°C | | Generator/ Blade | PMSM/3ea |

### 3.2 Experiment and results

A prototype for the proposed system has been built and experimentally tested, as shown in Fig. 16(a). The experimental conditions are wind speed (0-3[*m/s*]), insolation (400-800[$W/m^2$]), temperature (27.5[$^oC$]). Fig. 16(b) shows the controller with a low-cost micro controller and the battery.

The field test results are shown in Fig. 17. Fig. 17(a) shows the voltage from photovoltaic modules, wind generator, battery, and LED lighting. Fig. 17(b) shows their currents. The power output from each source of

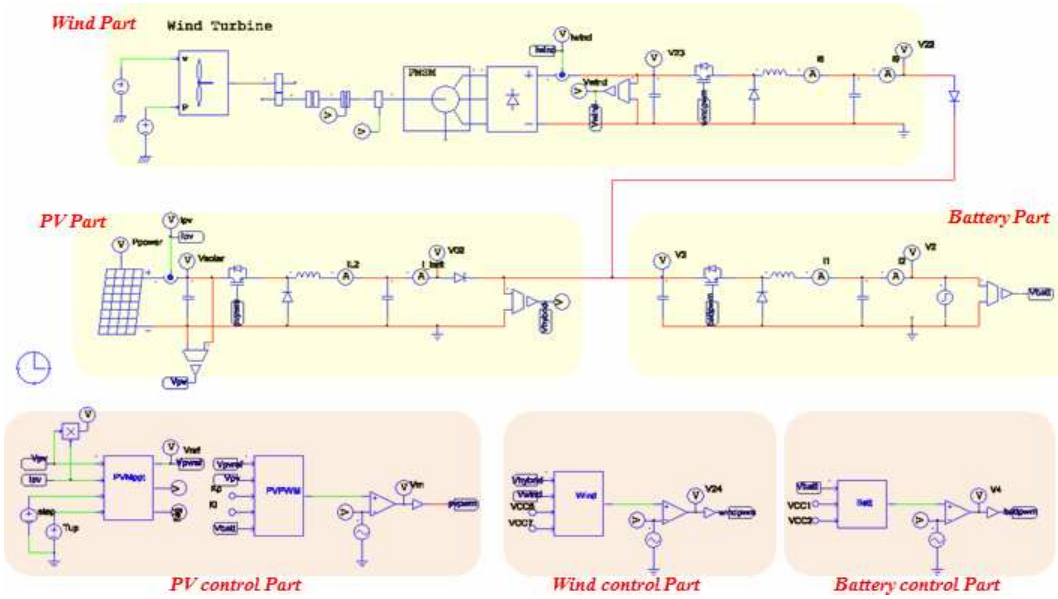


**Fig. 14.** Simulation of WP-HPS/Battery

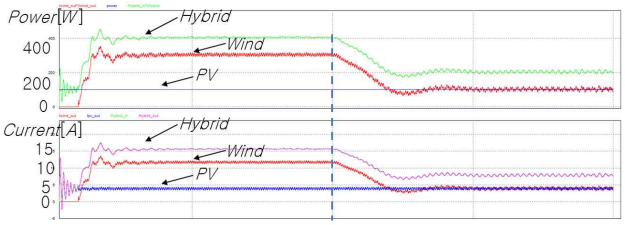


(a) Variable wind speed

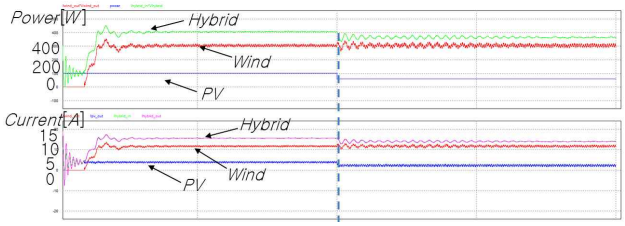


(b) Variable insolation

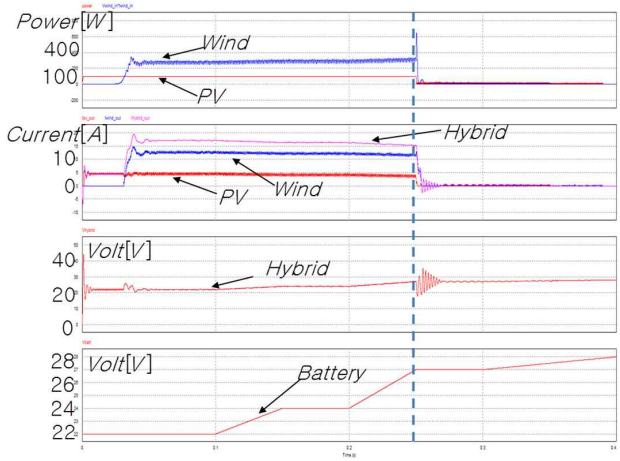


(c) Variable battery voltage

**Fig. 15.** Result of simulation

(a) Prototype

(b) Controller and battery

**Fig. 16.** Wind/Solar Hybrid Power System

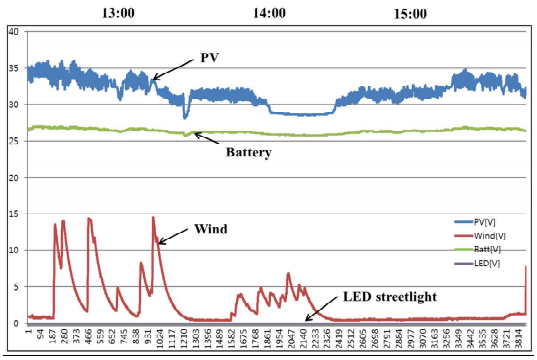


(a) Voltage characteristic

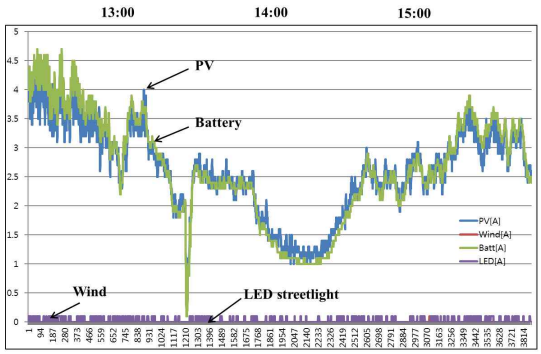


(b) Current characteristic

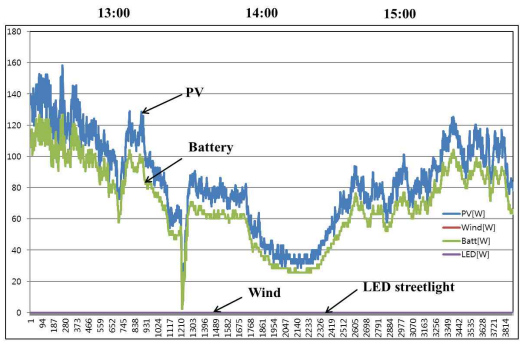


(c) Power characteristic

**Fig. 17.** Results of field test (day time)

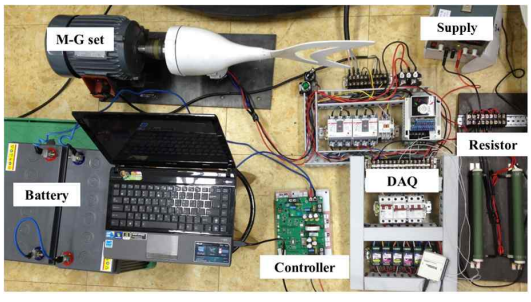


**Fig. 18.** Configuration of test bed

energy is plotted in Fig. 17(c). The photovoltaic controller was working in MPPT mode, tracking maximum power point of the photovoltaic modules. The output power of the photovoltaic modules increased with the solar insolation. The battery was charged because there was no load.

In the field test, the wind speed was very low. Therefore, as shown in Fig. 18, the test bed configured to input the wind speed. The speed of the wind generator combined

with an induction motor is controlled by inverter.

The experimental condition of this case is as follow; wind speed (8-10 [*m/s*]), insolation (400-600 [$W/m^2$]), temperature (27.5 [$^oC$]).

Fig. 19 shows the results of the WS-HPS in test bed. In this case, dual signal of wind power and solar power are input together. The photovoltaic power is controlled by MPPT since the wind generator power is higher than the photovoltaic power output. The wind generator voltage tracks the voltage of photovoltaic power. The charge of the battery by the dual input power is faster than in the field test (single input).

Fig. 20 shows the profile of the voltage and the power of the WS-HPS during the night (21:00-23:00). In this case the torque of the wind generator is controlled by an induction motor with a controller as the wind turbine emulator, as shown in Fig. 18. When starting the turbine, the wind voltage and power are gradually increased. Since the power of the wind system is less than that demanded by the LEDs in normal condition, the rest of the power is supplied by the battery. During the dimming, the power of the wind system is only delivered to the LED lighting.

Fig. 21 represents the average charging efficiency, which is 90.98[%]. The charging efficiency is the ratio of the charging power to the source power of the wind and solar systems.

Fig. 22(a) shows the LED lighting current, voltage, and PWM signal with around 60[%] duty cycle when the IR sensor is not activated. At this moment, the voltage is 17.1[*V*], and the current is 0.4[*A*]. Fig. 22(b) shows the LED voltage and current, and PWM signal with 98[%] duty cycle when the IR sensor is activated. The voltage is

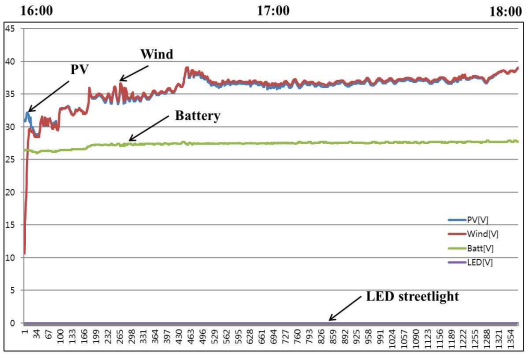


(a) Voltage characteristic

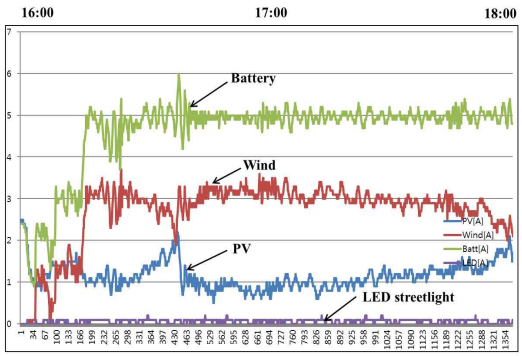


(b) Current characteristic

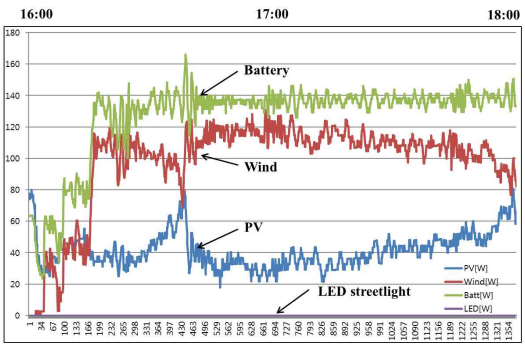


(c) Power characteristic

**Fig. 19.** Results of test bed (day time)

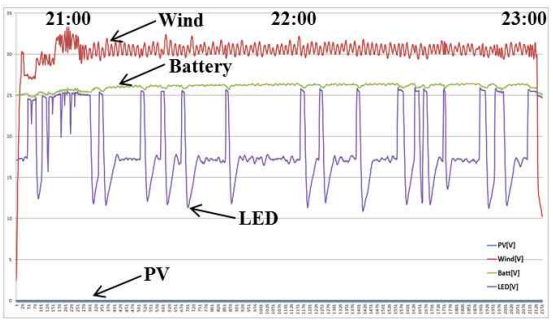


(a) Voltage characteristic

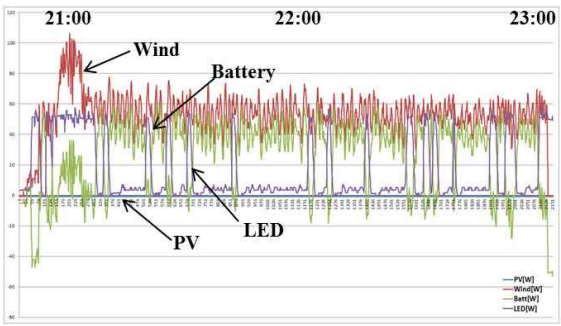


(b) Power characteristic

**Fig. 20.** Results of test bed (night time)

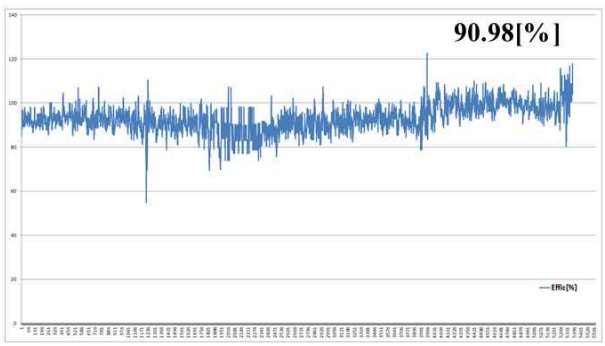


**Fig. 21.** Efficiency characteristic of WS-HPS

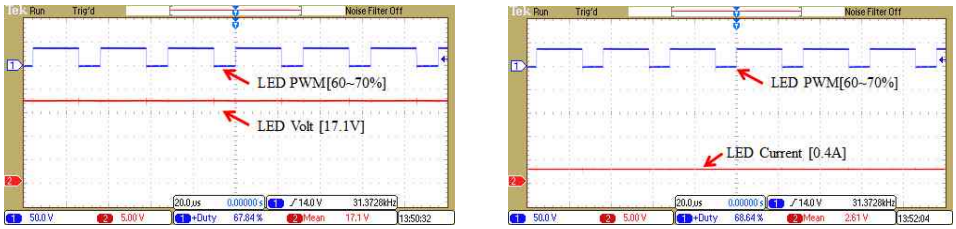


(a) Case I. IR sensor non detection (no motion)

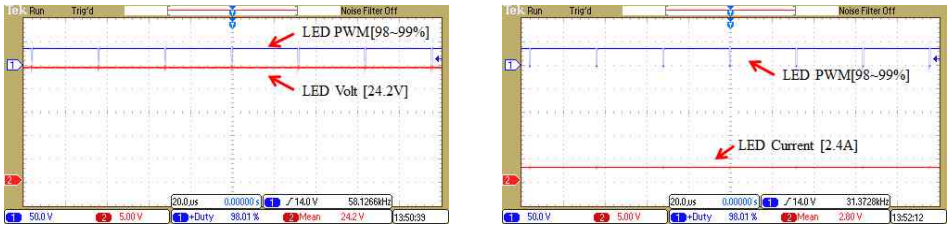


(b) Case II. IR sensor detection (motion)

**Fig. 22.** Output characteristics of LED lighting system

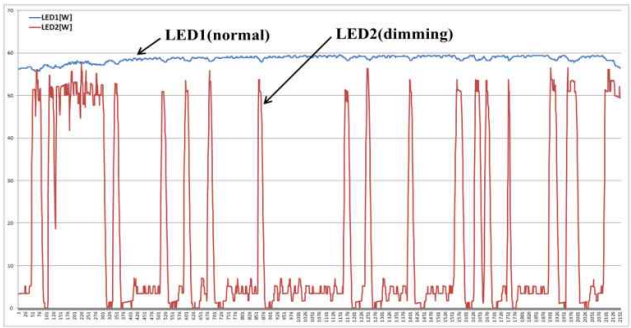


**Fig. 23.** The voltage of field test results of LED lighting system

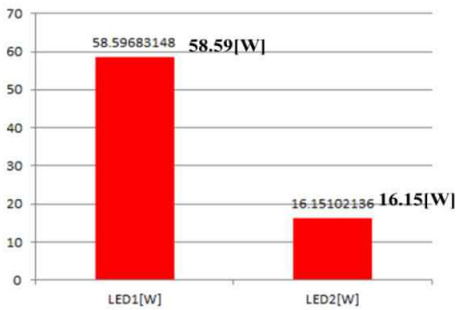


**Fig. 24.** The consumed power of the normal system and dimming system

24.2[*V*], and the current is 2.4[*A*]. If the current is lower than 0.4[*A*], flickering can be observed in the LED lighting. Fig. 23 shows the voltage of the field test results for 1 hour. As shown in Fig. 24, this method can reduce energy consumption by about 75[*%*] when the IR sensor is not activated. When the IR sensor was activated, the dimming control was initiated after 30[*sec*].

## 4. Conclusion

A proposed WS-HPS based LED street lighting system has been described. The system integrates new technologies and offers ease of maintenance and energy savings. In order to improve the performance and reduce cost of the system, the control strategy for charging and discharging, saving energy, and maintenance of the WS-HPS based LED street lighting system have been studied in detail.

The hybrid output power characteristics of the system have been analyzed by a field test, along with the battery charge/discharge characteristics and dimming characteristics of the LED lighting system. The developed controller is able to increase the power efficiency by tracking the maximum power of the wind-solar power system. Also, charge efficiency and life time of the battery are increased by three-step control. The power efficiency is increased by approximately 20[*%*] by dimming control of LED lighting system.

The proposed system will be made more applicable through continued experiments in various environmental conditions, such as mountainous areas, island, and standalone system.

## References

[1] Remus T., Marco L., Pedro R., "Grid Converters for Photovoltaic and Wind Power Systems", wiley, 2011.

[2] M. Engin, M. Colak, "Analysing solar-wind hybrid power generating system", Pamukkale University Faculty of Engineering, Journal of Engineering Sciences, Vol. 11, No. 2, pp. 225-230, 2005.

[3] Jicheng X., Huaquang Z., Zhixin W., "Research on Battery Charging Control Strategy in Stand-alone

Wind / Photovoltaic Hybrid Street Lamp Lighting System", Water Resources and Power, pp. 182-185, 2008.

[4] Caponetto R., Dongola G., Fortuna L., Riscica N., Zufacchi D., "Power consumption reduction in a remote controlled street lighting system" Power Electronics, Electrical Drives, Automation and Motion, SPEEDAM 2008, International Symposium on, pp. 428-433, 11-13 June 2008.

[5] Raymond A., Mack, Jr., "Demystifying Switching Power Supplies", ELSEVIER, 2004.

[6] V. Salas, E. Olias, A. Barrado and A. Lazaro "Review of the maximum power point tracking algorithms for stand-alone photovoltaic systems" Solar Energy Materials and Solar Cells vol. 90, Issue 11, 6 July 2006, pp 1555-1578.

[7] Y. Jung, J. So, G. Yu, and Ja. Choi. "Improved perturbation and observation method (IP&O) of MPPT control for photovoltaic power systems," Photovoltaic Specialists Conference, 2005. Conference Record of the Thirty-first IEEE , pp. 1788-1791, 3-7 Jan. 2005.

[8] Qiaoyun Z., Zhongdong Y., "Battery Energy Storage Research of Photovoltaic Power Generation System in Micro-gird", Critical Infrastructure(CRIS), 2010 5th International Conference, pp. 1-4, Sep. 2010.

[9] Zeng Wen-zian, Ma Jie, Zhai Ying, "Rapid Charge System for Lead-Acid Battery of Solar Energy Street Light based on Single-Chip Microcomputer", ICCSIT 2008, International Conference, pp. 337-341, 2008.

[10] Ali M., Qrabi M., Abdelkarim E., Qhaouq J.A.A, Aroudi A. E., "Design and development of energy-free solar street LED light system", 2011 IEEE PES Conference, pp. 1-7, 2011.

**Yong-Sik Lee** He received his B.S and M.S degrees in Electrical Engineering from Sunchon National University, Korea in 2008 and 2011, respectively. Currently, he is pursuing his Ph.D. degree in Sunchon National University.

**Jae-Hyeon Gim** He received his B.S. degree from Hongik University, Seoul, Korea in 1977, M.S and Ph.D degrees in Electrical Engineering from the University of Texas at Arlington, in 1989 and 1993, respectively. He is currently a professor in the Dept. of Electrical Engineering at Sunchon National University.